Andrijana Ćurković
Milan Ćurković ✉
Domagoj Samardžić

https://doi.org/10.21278/TOF.482058923
ISSN 1333-1124
eISSN 1849-1391

HIERARCHICAL SPLINE IN THE REPRESENTATION OF A MODEL WITH AN EXTREMELY ROUGH SURFACE

Summary

This paper presents the application of hierarchical splines on the representation of models with extremely rough surfaces. The displacement between the smooth spline and the rough shape is stored as a set of images, where the displacement scalar is approximated using all three channels of the image (red, green, and blue). This type of surface representation allows easy and fast scientific analysis, interactive web display, and a significant reduction in the size of the extremely rough shapes. By using hierarchical splines over B-spline in combination with a compact displacement representation, we aim to achieve the same displacement quality of the whole surface, taking care that the model does not require much memory and is suitable for fast rendering. The focus of the study is on models from cultural heritage, without diminishing the importance of applying the approach to models from other areas.

Key words: *hierarchical spline, displacement mapping, cultural heritage, downsizing memory space, rough surface*

1. Introduction

Recent advances in scanning technology have made it possible to obtain extreme detail from scanned models. Parallel to this progress, the number of applications of such models in various fields has also grown. In the film and gaming industries [1], there are requirements for fine facial details such as pores and scars that should also be part of the animations. The model to which the specified details belong must be suitable for animation and editing because the specified actions must be intuitive, simple, and user-friendly for artists. The same requirement for details also exists in medicine, where small tissue damage is observed on scanned 3D models. In computer graphics [1,2], the big problem is creating realistic 3D facial models because human faces are very sensitive to changes. Ocean modelling [3,4] includes seafloor approximations with a detailed model that allows for easy analysis. Scanned models of cultural heritage objects [5] pose a great challenge for scientific analysis due to the excessive density of the scanned form, whether it is artistic details on an exponent or accurate modelling of damage. For valuable artifacts that are exposed to external influences (e.g., sun, wind, and water), it is important to accurately track the development of damage in order to restore the objects (e.g., sculptures on cathedrals) to their original condition and, if necessary, adequately protect them from further erosion. Scanning museum exhibits enables large numbers of users to visit virtual

museums, making it necessary to transfer data in real time and even store large collections in one place. For all these reasons, there is a need for a model that faithfully presents the detailed scanned models, does not require much storage space, and is suitable for remodelling, animation, adaptive rendering, and scientific analysis. Such models already exist, and they are known in the literature as displacement surface models. In the following, some of them, which are most relevant to this study, are briefly presented. In [2], Aaron Lee et al. presented a model of displaced subdivision surfaces with a compact representation of offset from the smooth parametric model to the scanned 3D model. The main geometric information is stored as a parametric model, while the displacement is represented by a compact function of scalars. Dong et al. [1] present the synthesis of a face using multiscale face models. The synthesis is based on multilevel B-spline approximations of scalar displacements that are manually grouped and merged. Guskov et al. [6] present a surface displacement model called normal meshes. The authors made a parametric subdivision of the surface and stored the displacement as a scalar per vertex. Kermarrec et al. [7] used the Local Refinement B-spline (LR B-spline) surface approximation of coastal regions, where noisy and scattered point clouds are represented by a compact displacement surface model. The authors highlighted the advantages of LR B-splines over T-splines and hierarchical B-splines in this kind of application. Giannelli et al. [4] present Truncated Hierarchical B-splines (THB-splines) as a mathematical technology for adaptive refinement in geometric design and iso-geometric analysis and outline the application to seafloor approximations. Many other detailed surface models based on interpolation or spline approximation that do not rely on displacement can be found in modelling and animation [8–11], graphic design [12], and seafloor approximation [3,13]. As the global market for specialized products grows, so does the demand for highly customized products, posing a challenge for real-time data collection and feedback in manufacturing [14]. Improving image analysis can help automate customized manufacturing decisions that can be made based on image data.

We mainly apply the proposed model to diverse surfaces from the cultural heritage that has become the field of application of algorithms and techniques from the fields of information and communication technology, image processing, 3D visualization, 3D scanning, and modelling. The information about the smooth approximation of the model geometry is stored as a sparse mesh of control points of the parametric model, while the difference between the smooth model and the original model is stored as a two-dimensional scalar field, where the first two coordinates are known from the field topology, which is the key to reducing the data size. By using hierarchical splines over B-spline in combination with a compact displacement representation, we aim to achieve the same displacement quality of the whole surface, taking care that the model does not require much memory and is suitable for fast rendering. The first part of the proposed model relies on papers [15–17] describing a parameterization based on fitting parameter values and the classification of the 3D shape deviation using feature recognition operating on parameterized control points. Taken together, our main contributions to representing extremely rough shapes are as follows. The displacement is approximated using all three bitmap channels, which leads to an additional reduction in size compared to existing approaches; the model preserves a compact representation of the displacement of the entire model (set of images), which is required in many areas; the possibility of representing manifold surfaces by smooth connections between more THB splines; and the model allows the reuse of old models and comparison with new models only in certain regions.

The paper is organized as follows. The second section presents the proposed displacement surface model, outlining its various aspects. These include the use of B-spline as the first layer of the truncated hierarchical B-spline, the displacement approximation procedure, the coupling of THB-spline partitions at the first level while incorporating displacement, the refinement of the THB-spline with displacement, and the formulation of free surface topology and harmonic

mapping. The third section is focused on exploring possible improvements and directions for future work, while the fourth section provides a discussion of the material presented. Finally, the fifth section concludes the paper.

2. The proposed displacement surface model

To illustrate the process of creating the proposed displacement surface model, we use the cultural heritage surface shown in Fig. 1 as an example. The example on which the model is presented is chosen because of the challenging combination of smooth and different types of rough surfaces. Rough surfaces are represented by artwork (hair), damage (nose), and sudden surface changes (eyes). The model we outline here includes a smooth approximation to the scanned 3D surface and the displacement as a set of images that represent the difference between the scanned surface and the smooth parametric model in the direction of the normal. For now, we manually split the surface of the manifold into two partitions and fit the parametric B-spline model on both partitions (Fig. 1). After the fitting, we calculate the displacement values for both smooth B-spline models to the detailed scanned 3D model. Coupling the two B-spline displacement surfaces is the next step, while extending the B-spline to a THB-spline is the last step to create the proposed model.

2.1 B-spline as the first level of the THB-spline

The B-spline surface is defined by its control points, degrees of polynomials, and the set of knots as

$$C(u,v) = \sum_{i_0=0}^{n_0} \sum_{i_1=0}^{n_1} N_{i_0,p_u}(u) N_{i_1,p_v}(v) \boldsymbol{Q}_{i_0 i_1} \in \mathbb{R}^3, \tag{1}$$

where $n_0 + 1, n_1 + 1$ are the numbers of the control points, and $N_{i_0,p_u}(u)$ and $N_{i_1,p_v}(v)$ are the basic B-spline functions of degrees $p_u, p_v \in \mathbb{N}$ defined by

$$\begin{aligned} N_{i,0}(u) &= \begin{cases} 1, & \bar{u}_i \le u \le \bar{u}_{i+1} \\ 0, & else \end{cases}, \\ N_{i,p}(u) &= \frac{u-\bar{u}_i}{\bar{u}_{i+p}-\bar{u}_i} N_{i,p-1}(u) + \frac{\bar{u}_{i+p+1}-u}{\bar{u}_{i+p+1}-\bar{u}_{i+1}} N_{i+1,p-1}(u). \end{aligned} \tag{2}$$

The knots $\bar{u}_i \in [0,1]$, as part of the basic B-spline functions, are set as

$$\bar{\boldsymbol{u}} = \left\{ \underbrace{0, \dots 0}_{p+1}, \bar{u}_{p+1}, \dots, \bar{u}_n, \underbrace{1, \dots 1}_{p+1} \right\}, \left\{ \bar{u}_i = \frac{i}{n} \right\}_{i=p+1}^{n}. \tag{3}$$

The matrix $\boldsymbol{Q}$ given by

$$\boldsymbol{Q} = \begin{bmatrix} \boldsymbol{Q}_{00} & \cdots & \boldsymbol{Q}_{0n_1} \\ \vdots & \ddots & \vdots \\ \boldsymbol{Q}_{n_0 0} & \cdots & \boldsymbol{Q}_{n_0 n_1} \end{bmatrix} \in \mathbb{R}^{3(n_0+1)\times(n_1+1)} \tag{4}$$

presents control points. Considering the values of the knots, the parameters (u, v) belong to the domain $[0,1]\times[0,1] \subset \mathbb{R}^2$. Since the goal of the study is to ensure a homogeneous displacement of the entire surface and since we know that the surface topology has an impact on the fitting process and, in the end, on the distribution of the control points, it is important to generate an appropriate topology. In this study, we have considered two variants of surface topologies. The free surface form, as an original surface triangulated mesh, is the standard form used in the creation of parametric models. The equation below shows the error function in the case of fitting the B-spline model to the surface with the free surface form, where $\boldsymbol{v}_j \in \mathbb{R}^3$ represents the

vertices of the original surface triangulated mesh and (u_j, v_j) corresponds to a parametric value from the parametric domain $[0,1]\times[0,1] \subset \mathbb{R}^2$.

$$\boldsymbol{E}_{freeform}(\boldsymbol{Q}) = \frac{1}{2}\sum_{j=0}^{m}\left\|C(u_j, v_j) - \boldsymbol{v}_j\right\|^2 \tag{5}$$

By minimizing the above least squares error function, we obtain control points $\boldsymbol{Q}$. As will be shown in the free surface form topology and harmonic mapping subsection, the distribution of control points obtained using the above error function is too sensitive to the given topology of the parametric domain. To avoid this kind of sensitivity and to obtain a stable and expected distribution of control points, we prefer to use the matrix form of the topology, which assumes that the model surface is represented in the matrix form

$$\boldsymbol{V} = \begin{bmatrix} \boldsymbol{v}_{00} & \cdots & \boldsymbol{v}_{0m_1} \\ \vdots & \ddots & \vdots \\ \boldsymbol{v}_{m_0 0} & \cdots & \boldsymbol{v}_{m_0 m_1} \end{bmatrix} \in \mathbb{R}^{3(m_0+1)\times(m_1+1)}, \tag{6}$$

where m_0 is the number of sections, and m_1 is the number of vertices in each section. A detailed description of the matrix form of the surface can be found in [15–17]. The equation below represents the corresponding error function

$$\boldsymbol{E}_{matrix}(\boldsymbol{V}) = \frac{1}{2}\sum_{i_0=0}^{m_0}\sum_{j_0=0}^{m_1}\left\|C(u_{i_0 j_0}, v_{i_0 j_0}) - \boldsymbol{v}_{i_0 j_0}\right\|^2, \tag{7}$$

where $\left(u_{i_0 j_0}, v_{i_0 j_0}\right)$ are the parametric values from the parametric domain $[0,1]\times[0,1] \subset \mathbb{R}^2$ (Fig. 1b and c) associated with the vertex $\boldsymbol{v}_{i_0 j_0} \in \mathbb{R}^3$ from the matrix representation $\boldsymbol{V}$. The following examples in this study are generated based on the matrix form of topology. Figure 1 shows the result of B-spline fitting to two partitions of the scanned model, where harmonic mapping [18] into a parametric rectangular domain was applied to set the parametric values for each 3D model vertex.

a)

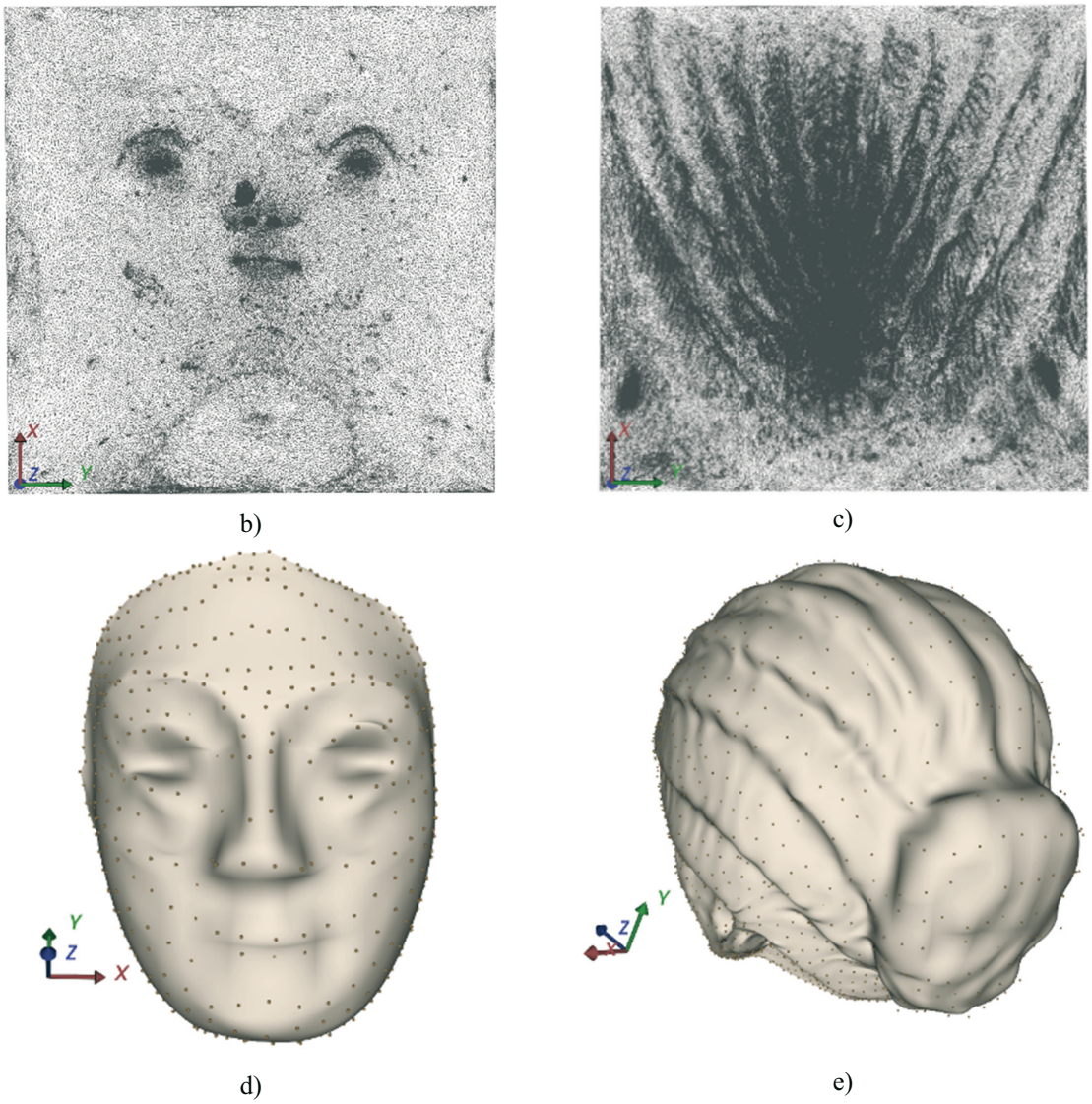

Fig. 1 B-spline fitted to the cultural heritage model obtained by a 3D scanning system: a) two partitions of the input model; b) and c) corresponding parametric projections; d) the B-spline model of the face with a 25×25 grid of control points; e) the B-spline model of the hair with a 48×48 grid of control points.

2.2 Displacement approximation

In this section, we assume that we have a smooth B-spline parametric model that fits the scanned 3D model. Instead of the extremely rough surface of the original model, the basic geometric information is stored as a parametric model defined with a coarse grid of 3D control points. Besides the ease of modelling geometry, the coarse grid of control points is one part of downsizing memory storage. The second key part of downsizing is the difference between the smooth parametric model and the rough surface of the input model, which is stored as a two-dimensional scalar field (single scalar per vertex), where two coordinates are known from the field topology. In the literature, there are models of displacement surfaces, and we highlight here the studies [2] and [1], which essentially coincide with our study. Compared to the mentioned studies, our model includes displacement approximation using three bitmap channels.

Based on experience and requirements from the cultural heritage field, we have a priory set grid size of $n_u \times n_v$ for the final displacement model. For samples in this study, we used $n_u = n_v = 1000$. We calculate parametric values for the B-spline model using the following formulation:

$$u_i = \frac{i}{n_u - 1}, i = 0, \dots, n_u - 1,$$
$$v_j = \frac{j}{n_v - 1}, j = 0, \dots, n_v - 1. \tag{8}$$

For each vertex $C(u_i, v_j)$ from the B-spline model, we calculate displacement to the original surface in the direction of the corresponding normal $\vec{\boldsymbol{n}}_{ij}$ on the parametric surface. Where a ray along the normal intersects the original mesh, there is a corresponding displacement point $\boldsymbol{S}_{ij}$. Normal $\vec{\boldsymbol{n}}_{ij}$ can be calculated using the Principal Component Analysis (PCA) algorithm for the neighbourhood of $C(u_i, v_j)$. For reasons of numerical simplicity and to avoid complex mathematical formulations for the derivation of the geometry, we have opted for a linear approximation of the geometry and computed the normal as the normalized sum of the normal of the adjacent triangles to the vertex $C(u_i, v_j)$ (Fig. 2 and Equation 9).

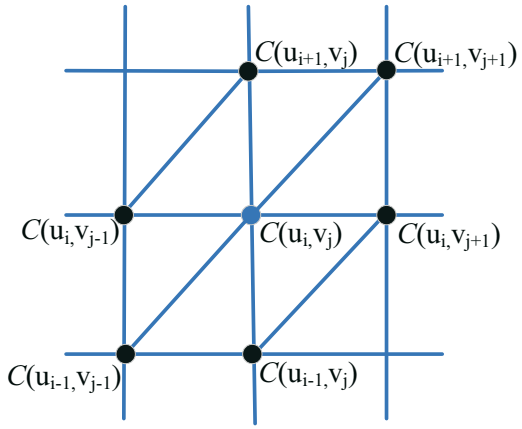

Fig. 2 The adjacent points/triangles to the point $C(u_i, v_j)$.

The interior normals are the sum of the six normals of a triangle;

$$\vec{\boldsymbol{n}}_{ij} = \sum_{i_o=i-1}^{i} \sum_{\substack{j_o=j-1 \\ (i_o,j_o)\neq(i,j-1)}}^{j} \left(C(u_{i_0+1}, v_{j_0}) - C(u_{i_0}, v_{j_0})\right) * \left(C(u_{i_0+1}, v_{j_0+1}) - C(u_{i_0}, v_{j_0})\right)$$
$$+ \sum_{i_o=i-1}^{i} \sum_{\substack{j_o=j-1 \\ (i_o,j_o)\neq(i-1,j)}}^{j} \left(C(u_{i_0+1}, v_{j_0+1}) - C(u_{i_0}, v_{j_0})\right) * \left(C(u_{i_0}, v_{j_0+1}) - C(u_{i_0}, v_{j_0})\right), \tag{9}$$

the normals at the edge are the sum of three normals of a triangle, the normals of the upper left and lower right angles are the normals of a single triangle, while the normals of the upper right and lower left angles are the sums of the normals of two triangles. After summation, each normal is normalized: $\vec{\boldsymbol{n}}_{ij} = \frac{\vec{\boldsymbol{n}}_{ij}}{\|\vec{\boldsymbol{n}}_{ij}\|}$. When displacement point $\boldsymbol{S}_{ij}$ is calculated as the ray section in the normal direction, the corresponding displacement value is defined by

$$d_{ij} = \left\|C(u_i, v_j) - \boldsymbol{S}_{ij}\right\| * \begin{cases} -1, & \vec{\boldsymbol{n}}_{ij} \cdot \left(C(u_i, v_j) - \boldsymbol{S}_{ij}\right) < 0 \\ 1, & \vec{\boldsymbol{n}}_{ij} \cdot \left(C(u_i, v_j) - \boldsymbol{S}_{ij}\right) \geq 0 \end{cases} \in \mathbb{R}. \tag{10}$$

Figure 3c shows a two-dimensional scalar array that contains the above displacement of the input 3D model and parametric B-spline model. The first two coordinates (u_i, v_j) of the displacement

of the surface are given by (8), and hence we only need to store displacement coefficients d_{ij}. Thus, for storing the displacement from Fig. 3c, we need 10^3 float values of four bytes. In the proposed displacement surface model, we decided to approximate a 32-bit scalar field (four bytes) with a 24-bit bitmap image to reduce the memory size. In what follows, we note the minimum displacement value by $minDisplacement$, and the maximum value by $maxDisplacement$. We scale each displacement d_{ij} from $[minDisplacement,\ maxDisplacement\ ]$ to $[0, 255\ ]$ and note that value by p_{ij} (Equation 11). Then, with the three following approximations, we store p_{ij} into 24-bit pixels, filling three channels: red, green, and blue.

$$p_{ij} = 255 * \frac{d_{ij} - minDisplacement}{maxDisplacement - minDisplacement}; \tag{11}$$

$$red_{ij} = int(p_{ij});$$

$$green_{ij} = int\left(255 * (p_{ij} - red_{ij})\right);$$

$$blue_{ij} = int\left(255 * (p_{ij} - green_{ij})\right).$$

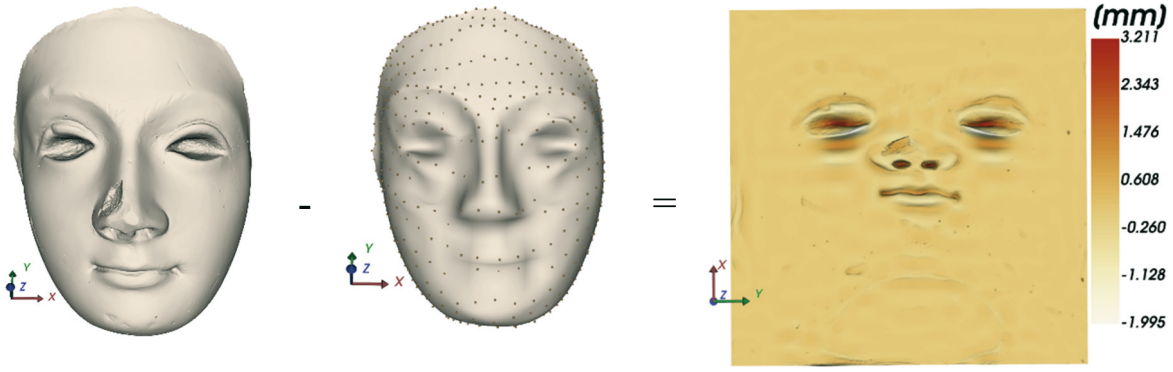

a) b) c)

Fig. 3 The proposed displacement surface as a scalar field: a) original model; b) parametric B-spline model with a grid of 25×25 control points; c) 1000 × 1000 scalar field as the difference of a) and b).

Figure 4 shows the final result of the approximation of the displacement with a 24-bit image. The image size corresponds to the grid size $n_u \times n_v$. In this way, we have reduced memory space by one byte per each displacement scalar d_{ij}.

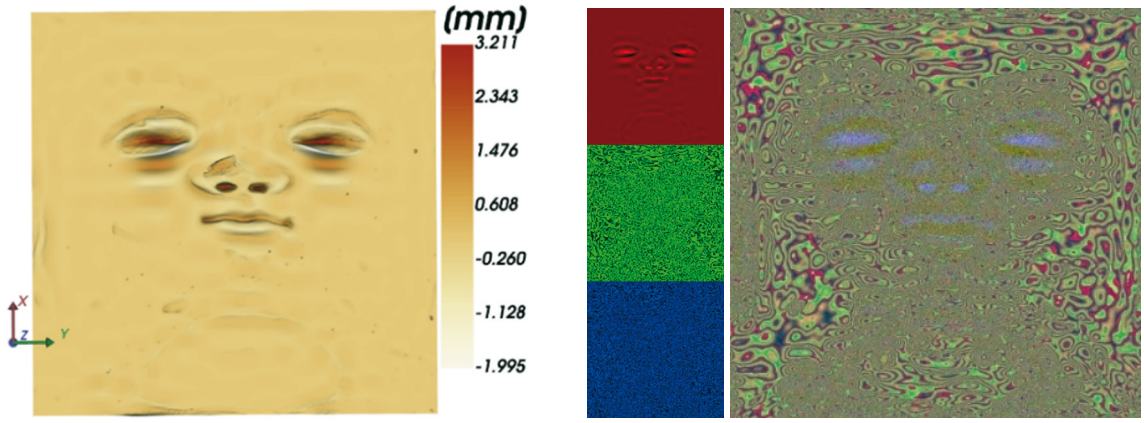

a) b)

Fig. 4 The approximation of the displacement scalar field with the 24-bit bitmap: a) the displacement field from Fig. 3; b) the approximation of a) with the 24-bit bitmap.

In this way, we have a simple displacement surface model consisting of a parametric B-spline model and a 24-bit bitmap in which the displacement coefficients are stored. Putting these two models together to form the final surface means that for each vertex $C(u_i, v_j)$, we need to calculate the normal $\vec{\boldsymbol{n}}_{ij}$ (Equation 9), and from the displacement bitmap, we need to calculate the displacement coefficient d_{ij}^{RGB} as the approximation of d_{ij} (10) using the following equations:

$$red_{ij} = \text{GetRedValue}\big(DisplacementImage(i,j)\big);$$

$$green_{ij} = \text{GetGreenValue}\big(DisplacementImage(i,j)\big);$$

$$blue_{ij} = \text{GetBlueValue}\big(DisplacementImage(i,j)\big); \tag{12}$$

$$d_{ij}^{RGB} = \Big(\big(red_{ij} + \big(green_{ij} + blue_{ij}/255\big)/255\big)/255\Big) * (maxDisplacement - minDisplacement) + minDisplacement.$$

We obtain the vertex on the final displacement surface by summing the vertex $C(u_i, v_j)$ from the parametric model and the corresponding normal $\vec{\boldsymbol{n}}_{ij}$ times the approximation of the displacement coefficient d_{ij}^{RGB}.

$$\boldsymbol{S}_{ij}^{RGB} = C(u_i, v_j) + d_{ij}^{RGB} * \vec{\boldsymbol{n}}_{ij}. \tag{13}$$

Figure 5 shows the final displacement surface models for both model parts.

In general, there is no limit to the resolution (number of 3D vertices) of a parametric model. The maximum resolution of the proposed displacement surface model is determined by the resolution of the 24-bit bitmap of the scalar displacement field, which is determined in advance. When viewing the model in the virtual museum, users can select a lower resolution to speed up rendering. This means that some rows and columns of the 24-bit bitmap of the scalar displacement field and the corresponding vertices of the parametric model are simply skipped.

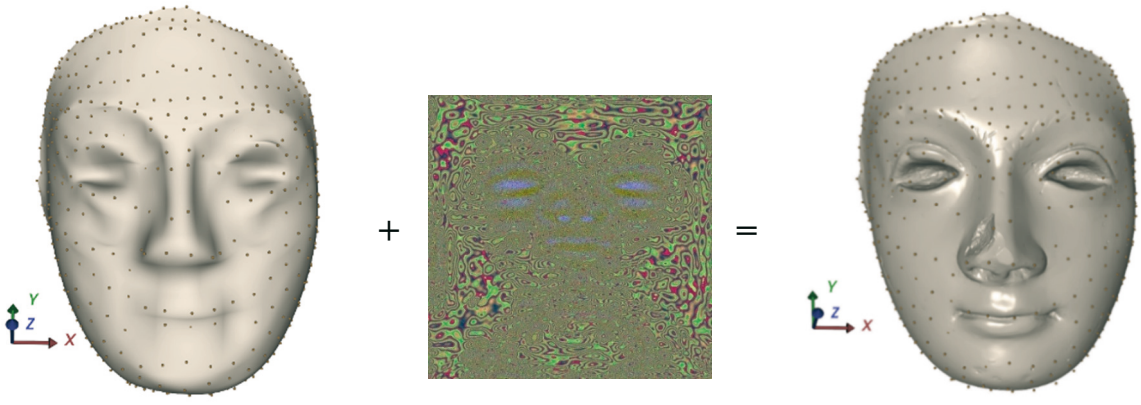

a) b) c)

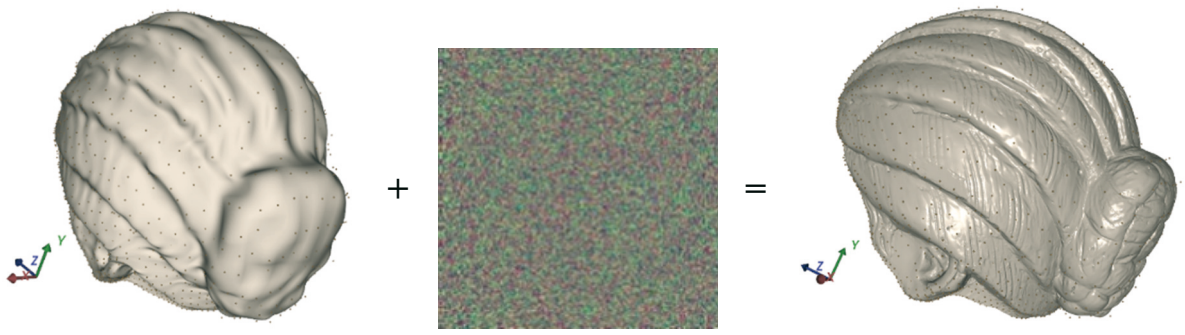

d) e) f)

Fig. 5 The proposed displacement surface model. The first column shows a parametric model; the middle column shows the displacement field as a 24-bit image; the third column shows a final $\boldsymbol{S}^{RGB}$ model. The parametric model of the face is a B-spline with a grid of 25×25 control points, while the parametric model of the hair is a B-spline with a grid of 48×48 control points.

2.3 Coupling of THB-spline partitions of the first level including displacement

In the previous section, we obtained two partitions (the face and the hair) of the proposed displacement surface model. If we put them together in the same coordinate system, they will be just two unconnected parts. To have a complete manifold displacement surface model, we need to connect them and achieve at least C^0 continuity in the boundary regions. Also, discontinuity should not be visible in the displacement details. To connect the partitions, we choose the size of the control point grid of both parts such that the knot vectors given by Equation (3) satisfy

$$\{\overline{\boldsymbol{u}}_{rare}\} \subseteq \{\overline{\boldsymbol{u}}_{dense}\},$$
$$\{\overline{\boldsymbol{v}}_{rare}\} \subseteq \{\overline{\boldsymbol{v}}_{dense}\}, \tag{14}$$

which, in our case, means $\{\overline{\boldsymbol{u}}_{face}\} \subseteq \{\overline{\boldsymbol{u}}_{hair}\}$ and $\{\overline{\boldsymbol{v}}_{face}\} \subseteq \{\overline{\boldsymbol{v}}_{hair}\}$. Figure 6 shows the proposed method of knot calculation in terms of smooth connectivity.

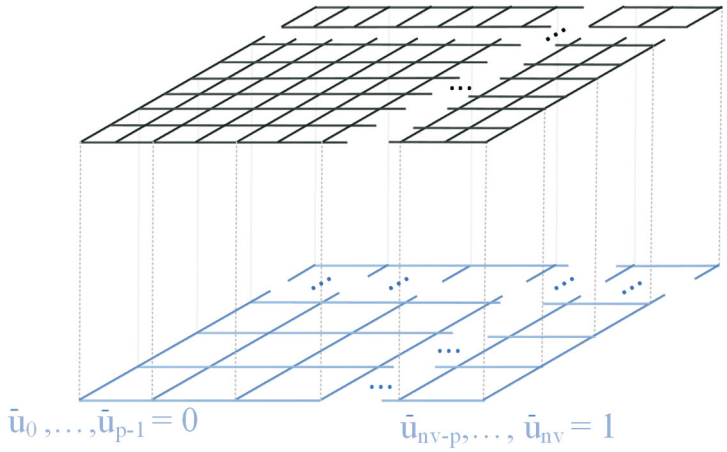

Fig. 6 The grid of knots in the case of the head model. The lower grid refers to the face knot vectors, while the upper grid refers to the hair knot vectors.

The second part of C^0 continuity lies in replacing boundary columns and rows of control points from the hair (denser) model with corresponding boundary columns and rows of control points from the face (coarser) model using the standard knot insertion algorithm, where we insert knots

from $\{\overline{\boldsymbol{u}}_{hair}\}$ that do not exist in $\{\overline{\boldsymbol{u}}_{face}\}$, and knots from $\{\overline{\boldsymbol{v}}_{hair}\}$ that do not exist in $\{\overline{\boldsymbol{v}}_{face}\}$. In this way, we keep the original geometry of rare boundary splines, and since the surface passes through boundary control points, we have C^0 continuity. If we want to have a higher level of continuity C^p on the boundary, we do the same for the p rows and columns of control points. Figure 7 shows the two parts of the proposed displacement surface model with C^0 continuity. The first part (face) is based on a grid of 25×25 control points, while the other one (hair) is based on a grid of 48×48 control points.

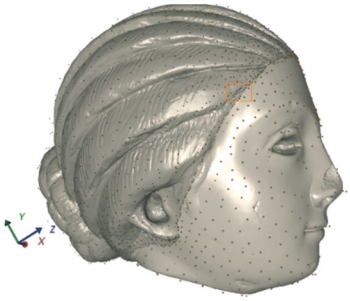

a)

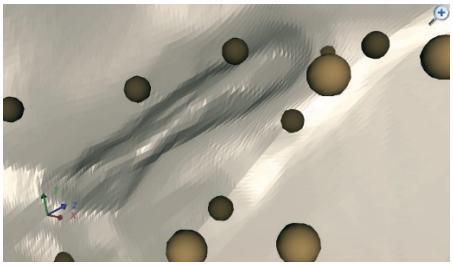

b)

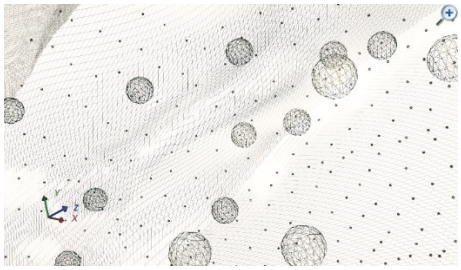

c)

Fig. 7 Coupling of two partitions of the proposed model of the displacement surface with C^0 continuity in the boundary area: a) the proposed model; b) and c) the zoomed section at the connecting boundary between the two partitions.

2.4 The refinement of the THB-spline with displacement

By combining the two partitions of the proposed displacement surface model with the corresponding continuity (Fig. 7), we have obtained a displacement surface model that largely meets the requirements we have in the cultural heritage field: fast transmission via the Internet, true-to-original representation, precise tracking of possible damage, and simple analysis. The details of the entire surface must be included in the proposed model without focusing on any particular part of the input surface. There is also the possibility for users to choose the resolution within the given limits ($n_u \times n_v$ is the maximum resolution). Still, there are examples that present challenges and that the proposed displacement surface model based on B-spline cannot describe with sufficient quality. Figure 8 shows two types of requirements that the proposed model should adequately meet. Both requirements refer to the change in the surface of the original model (Fig. 1a).

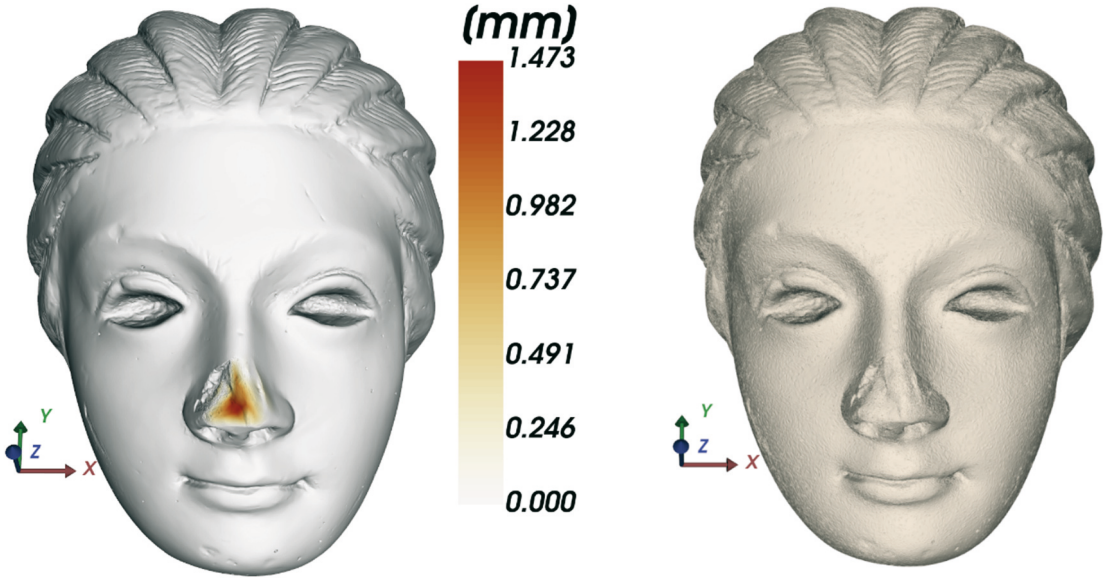

a) b)

Fig. 8 Surface damage compared to the original model surface: a) local damage with significant geometry changes and additional surface roughening; b) erosion of the entire model surface from a).

The first example (Fig. 8a) refers to the local damage to the surface compared to the input model (Fig. 1a). This type of damage may require additional fitting in this area due to geometric changes and the possible inability to accurately calculate displacement in normal directions. Furthermore, such localized damage (nose) may require a denser displacement surface than the surrounding surface (face). The problem of significant geometric changes in the nose area can be solved by the additional fitting of the entire face. The bigger problem is how to achieve a denser displacement surface in the same region. We can extend the maximum resolution $n_u \times n_v$ of the displacement 24-bit bitmap related to the entire face, but this is the case we want to avoid because of the large data space requirements. A simple solution to this problem is to use a hierarchical spline. We have chosen to upgrade the B-spline patch to a truncated hierarchical B-spline, which allows us to refine the corresponding parametric domain, resulting in a more faithful geometric representation. To increase the displacement density for the same subarea, we also calculate a separate 24-bit subdivision displacement map (Fig. 10). Here we outline a brief definition, while a detailed definition and extensive discussion of THB-splines can be found in [4,19,20], and the references therein. A THB-spline is constructed as follows: we denote the B-spline basis of level $l-1$ by B^{l-1}. The support of β is given by $supp\ \beta = \{x : \beta(x) \neq 0 \ \wedge x \in \Omega^0\}$. The truncation of $\tau \in spanB^{l-1}$ form the level $l-1$ represented in terms of B^l by $\tau = \sum_{\beta^l \in B^l} c_\beta \beta^l$ with respect to B^l, and Ω^l is defined by $trunc^l \tau = \sum_{\beta^l \in B^l, supp\ \beta^l \not\subseteq \Omega^l} c_\beta \beta^l$. Then the THB basis T is defined recursively:

1. Initialization
   $T^0 = B^0$
2. Recursion
   for $l = 1, \ldots, N$
   $T_A^l = \{trunc^l \tau : \tau \in T^{l-1} \wedge supp\ \tau \not\subseteq \Omega^l\}$
   $T_B^l = \{\beta^l \in B^l : supp\ \beta^l \subseteq \Omega^l\}$
   $T^l = T_A^l \cup T_B^l$

3. Result
   $T = T^N$

For the example in Fig. 8a, Fig. 9 shows the subdivision of the parametric domain.

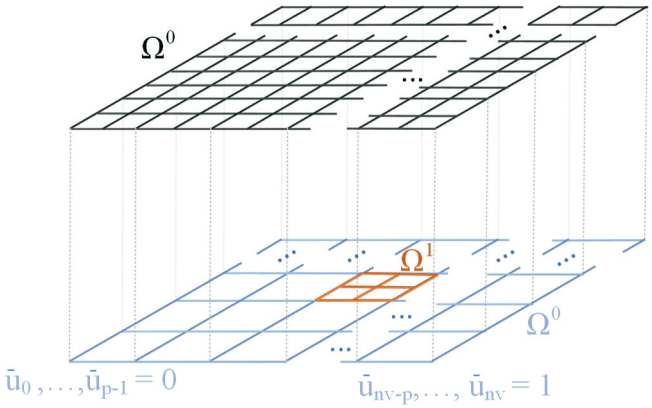

Fig. 9 The parametric domain and the corresponding knots. The lower subdivided grid refers to the face, while the upper grid refers to the denser hair grid.

Figure 10 shows the final displacement surface model where the face B-spline model has been upgraded to the THB-spline. Besides the more faithful geometric representation, Fig. 10b shows the sub-bitmap displacement image related to the nose area with a resolution of 500×500, resulting in a more detailed nose sub-area displacement surface.

The second type of surface damage (Fig. 8b) refers to the erosion of the entire model surface caused by weathering (wind, sun, and water) in cultural monuments. In this case, the question arises whether the old displacement surface model is able to describe the new small changes. We already have the THB subdivision of the nose area (Fig. 10a) and the 500×500 pixel displacement sub-image. For this part of the surface, we only need to recalculate the displacement sub-image as there is additional erosion. Due to additional erosion that has affected the entire model, the old resolution of the image of 1000×1000 pixels is not sufficient to faithfully represent the displacement of the face and hair. Therefore, we increased the resolution of the displacement image from 1000×1000 to 2000×2000 for each part, i.e., face and hair (Fig. 11). After increasing the resolution, the entire model displacement is represented with the same precision, without biasing any part of the surface. As a by-product of this action, the data space of the whole displacement model increased. The size of the original 3D scan data is approximately 700 MB, while the proposed model consists of a 25×25 control point grid for the face (50 KB), 16×8 control points for the nose region (20 KB), a 48×48 control point grid for the hair (62 KB), and three displacement images (6 MB); this takes a little more than 6 MB of memory in total.

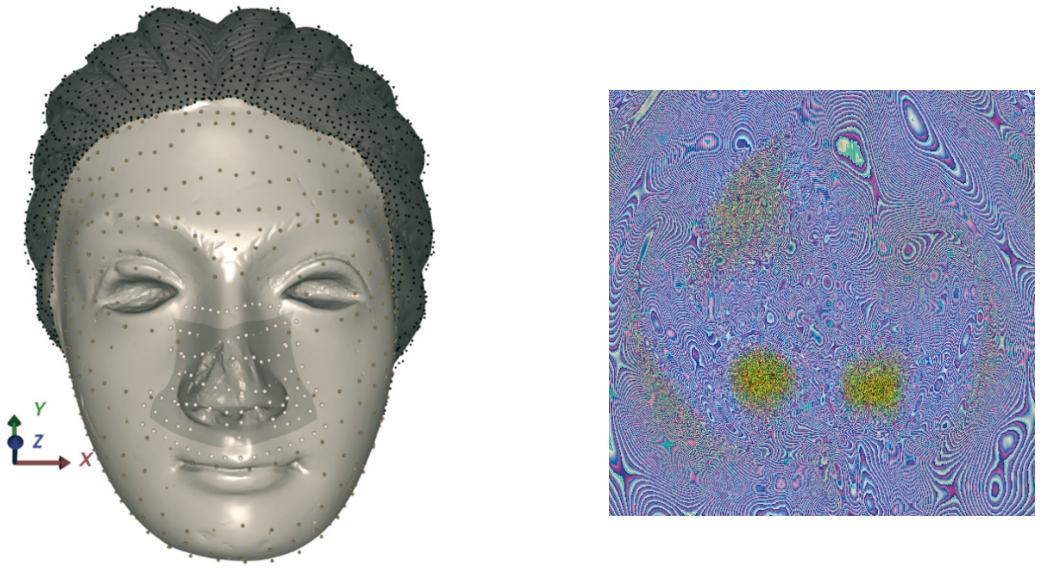

a) b)

Fig. 10 The proposed displacement surface: a) two connected displacement surfaces: hair based on B-spline and face surface based on THB-spline; b) displacement image related to the nose area with a resolution of 500×500 pixels.

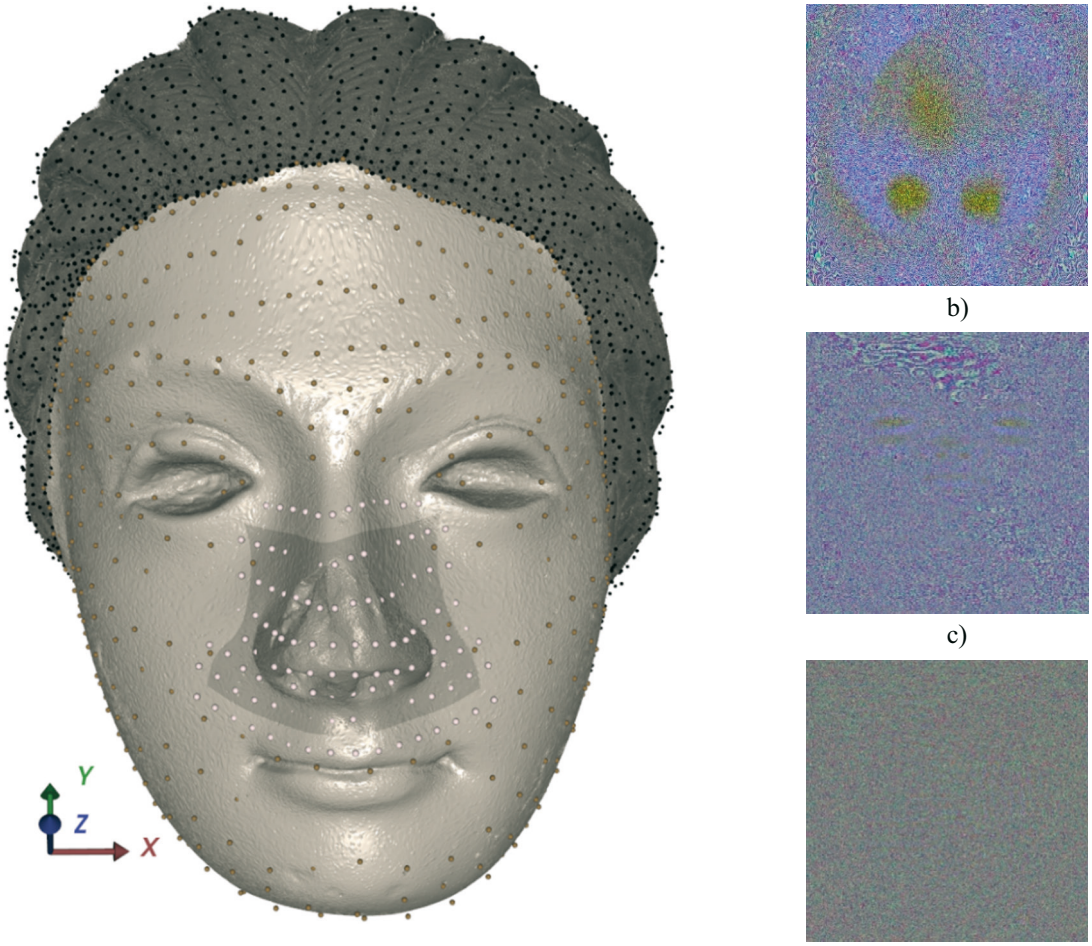

a) b) c) d)

Fig. 11 The proposed displacement surface: a) displacement surface of a model with an extremely rough surface; b) displacement image related to the nose area with a resolution of 500×500 pixels; c) displacement image related to the face with a resolution of 2000×2000 pixels; and d) displacement image related to the hair with resolution of 2000×2000 pixels.

2.5 Free surface form topology and harmonic mapping

The big challenge of the proposed model of displacement surface is to preserve the same quality of displacement for the entire surface without biasing any part of the surface. Besides the resolution of the displacement bitmap, the key point is the distribution of the control points of the parametric model. If we use the equidistant distribution of parameter values u_i and v_j according to Equation (8), more vertices $C(u_i, v_j)$ belong to the areas with dense control point distribution than to the areas with coarse control point distribution. For this reason, we have used the form of the matrix surface (6) instead of the free form of the surface (5) to preserve a more equidistant distribution of control points; this is necessary for an equal displacement representation of the entire surface. However, the matrix form also has disadvantages, namely additional computational effort and mesh topology for objects with abrupt geometry changes, which ultimately lead to an equidistant distribution of control points. In the following, we explain why we have avoided the free surface form at the moment and propose a solution to overcome the problems with the topology of the free surface form.

We need to map the surface S onto the plane rectangle D by flattening the surface and adjusting the boundary to the chosen shape ($[0,1]\times[0,1] \subset \mathbb{R}^2$). We start with the mapping $\Phi = (u, v)\colon \mathrm{S} \rightarrow \mathrm{D}$ that should minimize the stretching, i.e., preserve the ratio of the side lengths of the triangle on the surface S as much as possible. Minimizers of these functionals are harmonic functions, more precisely solutions of the Laplace equations $\Delta u = 0, \Delta v = 0$ on S with the Dirichlet boundary conditions $u = h_1, v = h_2$ on ∂S, where ∂S is the boundary of the surface and h_1 and h_2 are the given boundary mapping functions. By Rado's theorem, the harmonic mapping Φ is a bijective diffeomorphism if h_1 and h_2 are bijective homeomorphisms. Since the surface S is triangulated, this problem can be written in discrete form. Each point p inside the triangle can be written as a linear combination of vertices. Likewise, each value of $\Phi(p)$ can be written as a linear combination of the mapping values of Φ at the vertices. By direct calculation, it can be shown that the harmonic energy $E(\Phi)$ of the function Φ, representing the stretching, is equal to $E(\Phi) = \int_S \left|\nabla_g \Phi\right|^2 \mathrm{d}A = w_{ij}\left(\Phi(\boldsymbol{v}_i) - \Phi(\boldsymbol{v}_j)\right)^2$, where w_{ij} can be easily calculated by elementary mathematics if the gradient is calculated considering the Euclidean norm (see [18] for details). Figure 12a shows the distribution of geometric features computed by the principal component analysis algorithm, and Fig. 12e shows the parametric B-spline model where the above Euclidean coefficients w_{ij} were used for the surface mapping onto $[0,1]\times[0,1]$. In general, the distribution of control points depends on the geometry and the surface topology. While the geometry is predetermined and should not be changed, attention should be paid to the surface topology for an equidistant distribution of the control points.

To achieve a more equidistant distribution of control points while using the free form of the surface, we will allow stretching or shrinking in the area of the dominant geometric features. This can be achieved by adjusting the norm, i.e., changing the weight factors w_{ij}. This change induces the stretching or shrinking of a part of the surface. Namely, to the standard Euclidean norm weight coefficient, we added two types of terms. To stretch the area of dominant geometric features, we added $\left\|\boldsymbol{v}_i - \boldsymbol{v}_j\right\|^{10*\left(v_i^{eig} + v_j^{eig}\right)}$ (Fig. 12c) and to shrink the area of dominant geometric feature, we added $1/\left\|\boldsymbol{v}_i - \boldsymbol{v}_j\right\|^{10*\left(v_i^{eig} + v_j^{eig}\right)}$ (Fig. 12d), where v_i^{eig} relates to the ratio of eigenvalues from the PCA algorithm (Fig. 12a). The mapping Φ is determined as the solution of the discrete Laplace equations $\sum_{\boldsymbol{v}_j} w_{ij}\left(\Phi(\boldsymbol{v}_i) - \Phi(\boldsymbol{v}_j)\right) = 0$, for all interior vertices $\boldsymbol{v}_i$ and all $\boldsymbol{v}_j$ that are adjacent to $\boldsymbol{v}_i$.

Considering the influence of the correction of the weight coefficients on the relationship between the geometric features and the equidistant distribution of the parameter values, we believe that with the right stretching and shrinking operators, it is possible to achieve an equidistant distribution of the parameter values even for the freeform surface.

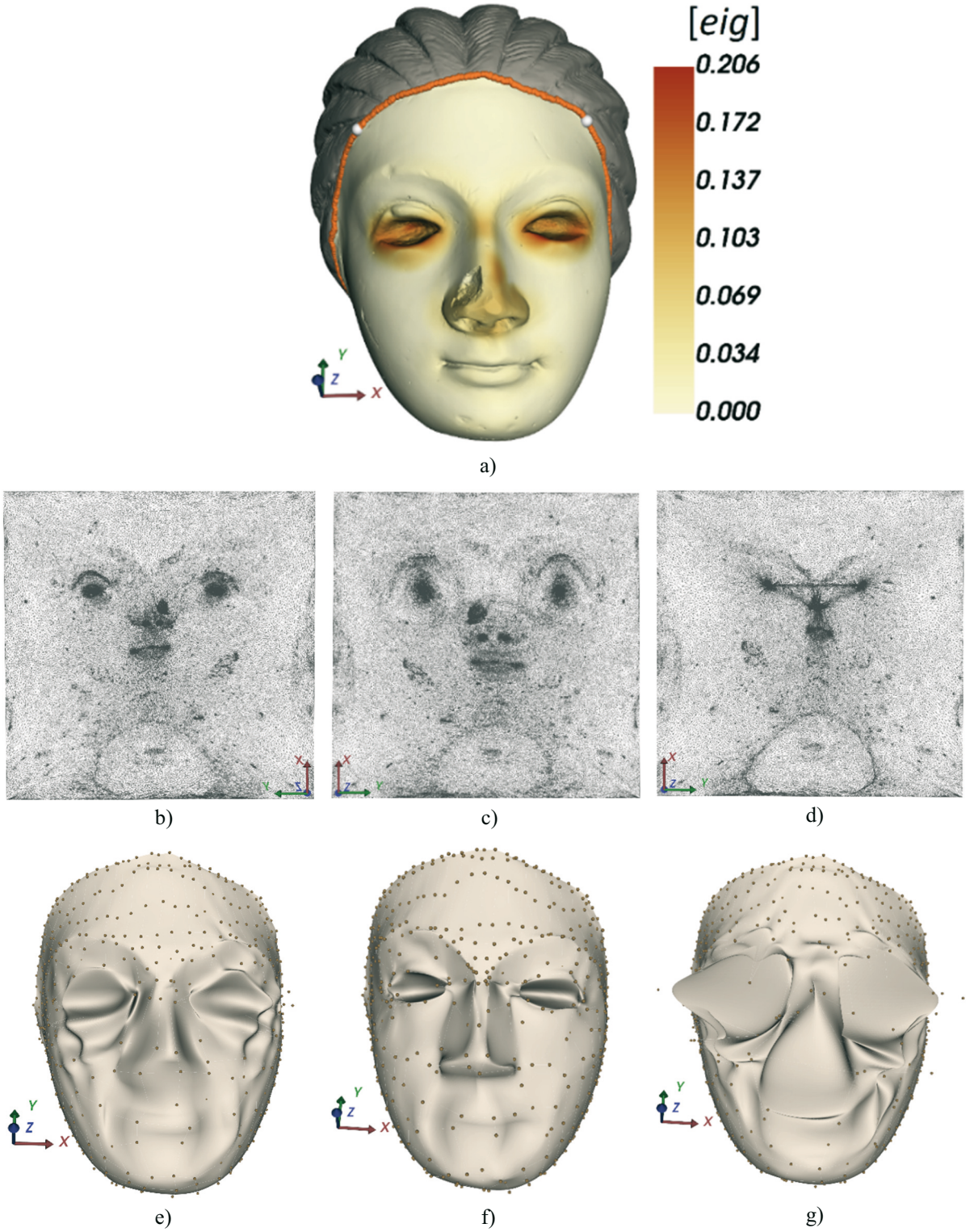

Fig. 12 The result of the proposed adaptation to the mapping function combined with the free surface form fitting (5): a) distribution of the geometric features calculated with the PCA; b) original harmonic mapping; c) mapping with the stretching operator included; d) mapping with the shrinking operator included; e) – g) B-spline models based on b) – d).

3. Future work

In future work, we will try to replace the matrix form of the surface with a free form. This will require additional effort to automate the settings of the shrink and stretch operators in mapping onto the parametric domain. Future work will also include the use of surface quadrangulation to avoid manual splitting of the scanned input model, resulting in a larger number of small partitions with separate displacement bitmap images. In this case, we expect the sensitivity to the given topology of the parametric domain to decrease, especially in the free surface form case.

4. Discussion

Displacement surface methods have been of interest to the scientific community for some time due to their applicability, and due to their complexity, not all application requirements have yet been met and progress is possible. The method proposed in this paper has similarities with the methods already proposed, but there are also innovations that have been introduced to obtain the best possible results for the cultural heritage example presented, as well as for other examples used during the research.

In paper [2], the authors presented a model for displaced subdivision surfaces with a compact representation of the displacement by a compact function of scalars. In this study, we used an approximation to the compact displacement representation using a 24-bit image, and for the surface subdivision, we used THB. In [1], which essentially coincides with our study, the authors present the synthesis of a face using multiscale face models. The synthesis of B-spline approximations of the surface and the displacement is the approach that exists in the proposed study, with the addition of THB subdivision and compact detailed displacement. The third paper relevant to the proposed study is [6], in which the authors present a similar model called normal meshes. The displacement is stored by one scalar per vertex, while the authors have made a parametric subdivision of the surface similar to the one we intend to use in our future work, but with a smaller number of quadrangular patches. In the publications [4] and [7], the authors present models of displacement surfaces in which a subdivision of the surface was made in order to obtain an accurate model, but in which (unlike the one we propose) there is no compact representation of the displacement offset compared to the original model.

Overall, the proposed model represents an advance in the additional downsizing of memory space by using three bitmap channels instead of scalars with real numbers and in the presentation of complex manifolds with a compact representation of the displacement.

5. Conclusion

Displacement surface models are becoming the standard models in many fields. Many requirements that these displacement surface models have to meet arise from these fields. They are: the small storage space of the model; easy reshaping and modification of geometry including displacement; the possibility of superimposing further displacements within the same model; the possibility of describing manifolds with included continuity; the possibility of describing extremely rough surfaces; easy scientific analysis, etc. There is no displacement surface model that can ideally fulfil all the above requirements. This is also the case with the proposed model, which is based on manual partitioning instead of automatic partitioning, which will be part of future work. On the other hand, the proposed model can describe a manifold with included continuity, it can describe extremely rough surfaces, it requires little memory space thanks to the approximation of the displacement by a 24-bit image, and it has the possibility of subdivision using the THB spline with a separate displacement sub-image if necessary.

Scientific analysis is very easy due to the compact representation of the displacement and the possibility of viewing the displacement over three images/channels. Superimposing further displacements is also easy to incorporate. Based on the above, we believe that our contribution will find a place in other applications and that other researchers will use it and, if possible, upgrade it.

REFERENCES

[1] Yoon S-H, Lewis J, Rhee T. Blending Face Details: Synthesizing a Face Using Multiscale Face Models. IEEE Comput Graph Appl. 2017;37:65-75. https://doi.org/10.1109/MCG.2017.4031069

[2] Lee A, Moreton H, Hoppe H. Displaced subdivision surfaces. Proc 27th Annu Conf Comput Graph Interact Tech - SIG13GRAPH '00. New York, New York, USA: ACM Press; 2000. p. 85-94. https://doi.org/10.1145/344779.344829

[3] Fu W, She J, Zhuang S. Application of an Ensemble Optimal Interpolation in a North/Baltic Sea model: Assimilating temperature and salinity profiles. Ocean Model. 2011;40:227-45. https://doi.org/10.1016/j.ocemod.2011.09.004

[4] Giannelli C, Jüttler B, Kleiss SK, Mantzaflaris A, Simeon B, Špeh J. THB-splines: An effective mathematical technology for adaptive refinement in geometric design and isogeometric analysis. Comput Methods Appl Mech Eng. 2016;299:337-65. https://doi.org/10.1016/j.cma.2015.11.002

[5] Ćurković M, Vučina D. PARAMETERIZATION OF COMPLEX CULTURAL HERITAGE SHAPES FOR ONLINE VIEWING AND INTERACTIVE PRESENTATION AND PROCESSING. Proc Arqueol 20 8th Int Congr Archaeol Comput Graph Cult Herit Innov. Valencia: Universitat Politècnica València; 2016. https://doi.org/10.4995/arqueologica8.2016.3510

[6] Guskov I, Vidimče K, Sweldens W, Schröder P. Normal meshes. Proc 27th Annu Conf Comput Graph Interact Tech - SIGGRAPH '00. New York, New York, USA: ACM Press; 2000. p. 95-102. https://doi.org/10.1145/344779.344831

[7] Kermarrec G, Skytt V, Dokken T. SURFACE APPROXIMATION OF COASTAL REGIONS: LR B-SPLINE FOR DETECTION OF DEFORMATION PATTERN. ISPRS Ann Photogramm Remote Sens Spat Inf Sci. 2022;V-2-2022:119-26. https://doi.org/10.5194/isprs-annals-V-2-2022-119-2022

[8] Zhang L, Snavely N, Curless B, Seitz SM. Spacetime faces. ACM Trans Graph. 2004;23:548-58. https://doi.org/10.1145/1015706.1015759

[9] Igarashi T, Nishino K, Nayar SK. The Appearance of Human Skin: A Survey. Found Trends® Comput Graph Vis. 2007;3:1-95. https://doi.org/10.1561/9781601980878

[10] Vrgoč A, Tomičević Z, Zaplatić A, Hild F. Damage Analysis in Glass Fibre Reinforced Epoxy Resin via Digital Image Correlation. Trans FAMENA. 2021;45:1-12. https://doi.org/10.21278/TOF.452024020

[11] Ćurković M, Udiljak T, Vuković-Obrovac J, Obrovac K. Application of white light interferommetry for foot orthotic design and manufacture. Trans Famena. 2009;33.

[12] Becker BG, Max NL. Smooth transitions between bump rendering algorithms. Proc 20th Annu Conf Comput Graph Interact Tech. New York, NY, USA: ACM; 1993. p. 183-90. https://doi.org/10.1145/166117.166141

[13] Hjelmervik JM, Barrowclough OJD. Interactive Exploration of Big Scientific Data: New Representations and Techniques. IEEE Comput Graph Appl. 2016;36:6-9. https://doi.org/10.1109/MCG.2016.53

[14] Salah B, Alsamhan AM, Saleem W, Khan R, Soliman ATA. 3D Simulation of a Yogurt Filling Machine Using Grafcet Studio and Factory IO: Realization of Industry 4.0. Transactions of FAMENA. 2023 47(3):15-30. https://doi.org/10.21278/TOF.473049922

[15] Ćurković M, Vučina D, Ćurković A. Enhanced 3D parameterization for integrated shape synthesis by fitting parameter values to point sets. Integr Comput Aided Eng. 2017;241-260. https://doi.org/10.3233/ICA-170541

[16] Vučina D, Ćurković M, Novković T. Classification of 3D shape deviation using feature recognition operating on parameterization control points. Comput Ind. 2014;65:1018-31. https://doi.org/10.1016/j.compind.2014.04.001

[17] Ćurković M, Ćurković A, Vučina D. Novel re-parameterization for shape optimization and comparison with knot-based gradient fitting method. Comput Methods Appl Mech Eng. 2018;336:304-32. https://doi.org/10.1016/j.cma.2018.03.018

[18] David Gu. Harmoic Map Tutorial [Internet]. 2023 [cited 2023 Nov 7]. Available from: https://www3.cs.stonybrook.edu/~gu/tutorial/HarmonicMap.html

[19] Giannelli C, Jüttler B, Speleers H. THB-splines: The truncated basis for hierarchical splines. Comput Aided Geom Des. 2012;29:485-98. https://doi.org/10.1016/j.cagd.2012.03.025

[20] Xie X, Wang S, Wang Y, Jiang N, Zhao W, Xu M. Truncated hierarchical B-spline-based topology optimization. Struct Multidiscip Optim. 2020;62:83-105. https://doi.org/10.1007/s00158-019-02476-4

Submitted: 19.9.2023

Accepted: 09.11.2023

Andrijana Ćurković
Faculty of Science, University of Split, Split, Croatia
Milan Ćurković*
Domagoj Samardžić
FESB, Faculty of Electrical Engineering, Mechanical Engineering, and Naval Architecture, University of Split, Split, Croatia
*Corresponding author:
milan.curkovic@fesb.hr